Available at www.sciencedirect.com

ScienceDirect

journal homepage: www.elsevier.com/locate/he

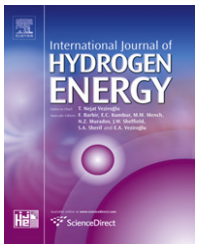

Experimental investigation of chemical-looping hydrogen generation using Al_2O_3 or TiO_2-supported iron oxides in a batch fluidized bed

*Shiyi Chen, Qiliang Shi, Zhipeng Xue, Xiaoyan Sun, Wenguo Xiang**

School of Energy and Environment, Southeast University, Nanjing 210096, China

ARTICLE INFO

Article history:
Received 20 February 2011
Received in revised form
21 April 2011
Accepted 26 April 2011
Available online 25 May 2011

Keywords:
Chemical-looping hydrogen generation
Hydrogen
CO_2 separation
Oxygen carrier
Iron oxide

ABSTRACT

Chemical-looping hydrogen generation (CLHG) is a novel technology for hydrogen production with inherent separation of CO_2. Three oxygen carriers Fe_2O_3 using inert materials Al_2O_3 or TiO_2 as support were prepared by mechanical-mixing method, i.e., Fe90Al10 (90%Fe_2O_3 + 10%Al_2O_3), Fe60Al40 (60%Fe_2O_3 + 40%Al_2O_3) and Fe60Ti40 (60% Fe_2O_3 + 40%Al_2O_3). Reactivity of the three oxygen carriers was first determined under CO reduction, steam oxidation and air oxidation atmospheres at 900 °C in a thermogravimetric analyzer. Then experiments to simulate the CLHG process were carried out in a batch fluidized bed. In the fluidized bed, all of the three oxygen carriers showed good reactivity over the multi-cycle experiments at 900 °C, and Fe60Al40 had the highest hydrogen yield. The reactivity of the oxygen carrier supported on Al_2O_3 was higher than that on TiO_2, which interacted with iron oxide forming $FeTiO_3$. The reactivity of Fe60Al40 was better than that of Fe90Al10. No deterioration of the oxygen carrier occurred after the multiple cycles, but for Fe90Al10 some agglomeration was detected. At 600–900 °C, higher temperature favored deeper reduction of iron oxide and increased the hydrogen production, while carbon deposition in the reduction period was suppressed with the rise of temperature. In the reduction, the conversion of fuel gas was constrained by thermodynamics in a single-stage reactor, and a compact fuel reactor was proposed for a full conversion of gaseous fuels.

1. Introduction

Hydrogen is expected to be the most important energy carrier in the next decades. It is clean and has almost no negative impact on the environment, because its combustion product is water. Although hydrogen is the most abundant element in the universe, it does not naturally exist in its elemental form on the earth. Pure hydrogen must be produced from other hydrogen-containing compounds such as fossil fuels, biomass, or water. Natural gas based steam-methane reforming is the predominant way of hydrogen production [1]. Coal, the most carbon-rich and therefore potentially the most polluting carbonaceous fuel, remains relatively abundant, and proven reserves are likely to last around 119 years at current rates of consumption [2]. Coal gasification is also an important method for hydrogen generation [3,4]. However, the hydrogen generation by reforming or gasifying carbonaceous fuels results in the emission of carbon dioxide. Carbon dioxide is the primary anthropogenic greenhouse gas which leads to global climate change in recent years. In order to use

* *Corresponding author*. Tel.: +86 25 8379 5545; fax: +86 25 8771 4489.
E-mail address: wgxiang@seu.edu.cn (W. Xiang).

0360-3199/$ – see front matter
doi:10.1016/j.ijhydene.2011.04.204

carbonaceous fuels directly for energy, or indirectly for hydrogen production, the development of carbon capture and storage technology will be essential.

Chemical-looping combustion (CLC) is a developing combustion technology with inherent separation of carbon dioxide. It is composed of two reactors, a fuel reactor and an air reactor. The solid circulating between the two reactors is called oxygen carrier, Me_xO_y, which is usually a metal oxide. The carbonaceous fuel is introduced to the fuel reactor where it reacts with oxygen carrier according to:

$$(2n + m)Me_yO_x + C_nH_{2m} \rightarrow (2n + m)Me_yO_{x-1} + mH_2O + nCO_2$$

At full conversion of the fuel gas, the outlet stream gases from the fuel reactor are only carbon dioxide and steam vapor. After water condensation, pure carbon dioxide can be obtained. The reduced metal oxide flows to the air reactor where it is reoxidized according to:

$$Me_yO_{x-1} + 0.5O_2 \rightarrow Me_yO_x$$

The flue gas from the air reactor is called oxygen depleted air which contains nitrogen and unreacted oxygen. The net reaction in CLC is the fuel combustion in the air, but with inherent separation of carbon dioxide. The studies on CLC have been widely carried out and the process has been successfully demonstrated using gaseous or solid fuels with different oxygen carriers [5–10]. In the past few years, a lot of work has focused on the development of oxygen carrier materials suitable for CLC [11,12]. An important characteristic of a successful oxygen carrier is its reactivity in both reduction and oxidation cycles. It must completely combust a fuel to achieve maximum fuel combustion efficiency. Additionally, the oxygen carrier must be resistant to mechanical and chemical deterioration by attrition, agglomeration, fragmentation, composition changes in the long term operation. The metal oxide proposed as potential oxygen carriers are NiO, Fe_2O_3, Mn_3O_4 and CuO while suitable supports are SiO_2, TiO_2, ZrO_2, Al_2O_3, YSZ and bentonite [12].

Since coal is the most abundant carbonaceous fuel in the world, recent research is aiming to adapt this technology to solid fuels. However, in solid fuels application, the slow step for gasification of char significantly decreases the overall fuel conversion rate in the fuel reactor. Thus, chemical-looping with oxygen uncoupling (CLOU) has been proposed as an alternative to CLC for solid fuels [13–16]. CLOU has a similar reactor layout as CLC. It involves three steps in the two reactors. In the air reactor a metal oxide captures oxygen from the air; in the fuel reactor the metal oxide decomposes to a reduced metal carrier and releases gas-phase oxygen; finally the gas-phase oxygen reacts with solid fuels. The thermodynamic-suitable oxygen carriers identified are CuO, Mn_2O_3 and Co_3O_4 [14]. Taking CuO as an example, in the fuel reactor, CuO decomposes to Cu_2O and releases oxygen O_2 at high temperature; the oxygen O_2 then combusts with the solid fuels and the gas product is mainly CO_2. In CLOU the intermediate gasification step is avoided and the char reacts directly with the gas-phase oxygen O_2. Mattisson et al. [14] presented the reaction rate of petroleum coke was approximately 50 times higher using CLOU compared to the reaction rate of the same fuel with an iron-based oxygen carrier in normal CLC.

Chemical-looping reforming (CLR) is also a technology developed from CLC [17–22]. In the case of partial conversion of methane using CLC, the flue gas from the fuel reactor is mainly comprised of CO and H_2. CLR is evolving as a technology for syngas production from natural gas and light hydrocarbons. It was proposed by Mattisson and Lyngfelt [23]. The basic principle of CLR is the same as CLC; however, the target product is not heat but syngas. It is important to select an oxygen carrier that tends to partially oxide methane to syngas rather than CO_2 and H_2O. In addition, the air to fuel ratio is kept low to prevent the full oxidation of the fuel [19]. The suitable oxygen carrier for CLR is NiO [17,19,24] due to its strong catalytic properties. Cerium oxide is also a candidate proposed for CLR [25], while oxygen carriers based on Fe_2O_3, Mn_3O_4 and CuO are not suitable [26] because these oxygen carriers suffer from poor selectivity to CO and H_2, with unreformed CH_4 leaving the reactor.

Besides CLR, there are suggestions that chemical looping can be applied to generate hydrogen directly [27,28], i.e. chemical-looping hydrogen generation (CLHG). The proposed routine is as follows: a metal oxide is reduced in the fuel reactor by gaseous fuels such as syngas or natural gas; the reduced metal oxide then reacts with steam in an oxidizing reactor, producing hydrogen. Compared with CLC, the air reactor in CLC is substituted by a steam reactor to yield hydrogen. Through this cycle, hydrogen is generated with inherent separation of CO_2. However, most of the oxygen carriers suitable for CLC or CLR are not appropriate to be applied in direct hydrogen generation. For example, it is very difficult for Ni and Cu to react with steam to produce hydrogen gas in thermodynamics [29–31]. Kang et al. [32] made a thermal analysis of chemical-looping process for hydrogen production and Fe_2O_3, WO_3 and CeO_2 were identified as suitable oxygen carriers. Fan et al. called this chemical-looping hydrogen generation process syngas redox (SGR) and syngas chemical looping (SCL) [33–36]. They evaluated the metal oxides of Ni, Cu, Cd, Co, Mn, Sn and Fe through experiments and found that Fe_2O_3 was the best candidate. Other oxides provide high conversion of syngas but lacks in producing hydrogen from steam. Veser et al. [37] called this process chemical-looping steam reforming (CLSR) and also screened that iron oxide was the best oxygen carrier. Thus, in view of thermodynamic equilibrium, melting point, chemical stability, toxicity and cost, iron oxide is the most potential oxygen carrier candidate used for CLHG.

In fact, the principle of CLHG using iron oxide as oxygen carrier to produce hydrogen is the steam-iron process. The steam-iron process was an old method for commercial hydrogen production in the early 1900s [38], but the traditional steam-iron process mainly focused on hydrogen production and could only partially convert the reducing gas [35]. Now, the steam-iron process is not used for hydrogen production because other technologies such as steam-methane reforming are more efficient. However, in recent years, CLHG is developed as a novel technology for hydrogen generation especially with inherent carbon dioxide capture. Thus, CLHG does not only focus on hydrogen generation but also on carbon dioxide capture. The looping in CLHG is similar to CLC

but there are some differences. Because of the special chemical characteristics of the iron oxide, the layout of reactors in CLHG needs to be changed. CLC and CLR use normally two interconnected fluidized bed reactors. However, CLHG with iron oxide as oxygen carrier consists of three reactors, a fuel reactor, a steam reactor and an air reactor, as shown in Fig. 1. In the fuel reactor, the oxygen-rich state hematite Fe_2O_3 is reduced to the oxygen-lean state wüstite FeO or metallic iron Fe by fuel gas (syngas as an example):

$$3Fe_2O_3 + CO \leftrightarrow 2Fe_3O_4 + CO_2$$

$$3Fe_2O_3 + H_2 \leftrightarrow 2Fe_3O_4 + H_2O$$

$$Fe_3O_4 + CO \leftrightarrow 3FeO + CO_2$$

$$Fe_3O_4 + H_2 \leftrightarrow 3FeO + H_2O$$

$$FeO + CO \leftrightarrow Fe + CO_2$$

$$FeO + H_2 \leftrightarrow Fe + H_2O$$

Ideally, the flue gas from the fuel reactor contains only carbon dioxide and steam vapor. Pure carbon dioxide can be obtained after water condensation. The reduced wüstite FeO or metallic iron Fe is then led to the steam reactor and oxidized to magnetite Fe_3O_4 by steam, producing hydrogen:

$$3Fe + 4H_2O \leftrightarrow Fe_3O_4 + 4H_2$$

$$3FeO + H_2O \leftrightarrow Fe_3O_4 + H_2$$

In the air reactor, Fe_3O_4 is subsequently regenerated to Fe_2O_3 by oxidizing oxygen in air:

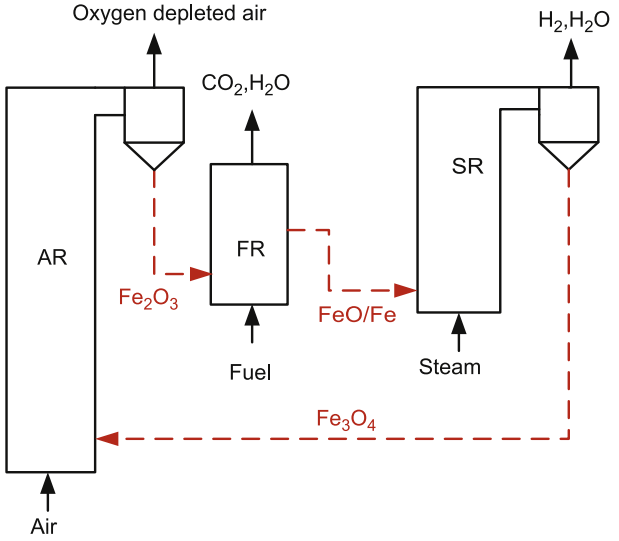

Fig. 1 – Conceptual scheme of three reactors CLHG.

$$2Fe_3O_4 + 0.5O_2 \leftrightarrow 3Fe_2O_3$$

The net reaction in CLHG is:

$$Fuel + H_2O + O_2 \rightarrow H_2 + CO_2$$

Bohn et al. [39] simulated CLHG in a packed bed and obtained hydrogen suitable for use in fuel cells (<25 ppm vol CO). It was suggested that the further reduction of FeO to Fe in the reduction phase was not recommended, because the reactivity of the iron oxide went bad after ten cycles. Cleeton et al. [40] investigated the reduction of Fe_2O_3 in the mixture of $N_2 + CO + CO_2$ in a fluidized bed at 850 °C and oxidation of the solids back to Fe_3O_4 in a $H_2O + N_2$ mixture, with the subsequent yield of hydrogen during oxidation being of interest. It was found that for the Fe_3O_4-Fe transition, the performance of the mechanically-mixed particles was extremely poor from the second cycle whilst all of co-precipitated samples produced consistently high hydrogen yields over 6 cycles. Li et al. [34] investigated the particles of iron oxide prepared using a sol-gel method, the solids showed a high reactivity, recyclability and low attrition rate. Yang et al. [41] successfully used char as a reducing material to reduce Fe_2O_3 to FeO and Fe for later hydrogen generation. Kierzkowska et al. [42] prepared composite particles Fe_2O_3 with Al_2O_3 using sol-gel method and $FeO{\cdot}Al_2O_3$ was detected after cycles; Chen et al. [43] found carbon dioxide in the fuel gas decreased the extent of iron oxide reduction and diminished the hydrogen yield in the later steam oxidation period. Chemical-looping hydrogen generation process can be integrated with combined cycle. Lozza et al. [44,45] proposed a natural gas fueled CLHG system for hydrogen and power generation and discussed the potential of the process. The system net LHV efficiency exceeded 51% with liquid, sequestration-ready CO_2 and negligible NO_x emissions. Xiang et al. [46] also modeled the combined cycle, and found an electricity efficiency of 10.13% and a hydrogen efficiency of 41.51% without CO_2 emission could be achieved when supplementary firing was not used. Compared with CLC, CLHG has two major differences.

(1) Thermodynamic analysis for CLC predicted by Mattisson et al. [47] showed that complete combustion of fuel to carbon dioxide and steam was only achieved when hematite Fe_2O_3 was partially reduced to magnetite Fe_3O_4. But in CLHG, the reduced solid of iron oxide is wüstite FeO or metallic iron Fe for later hydrogen generation;
(2) In CLHG, there is a steam reactor, and the partial pressure of steam will be high enough to overcome the equilibrium to generate hydrogen. Thus, it is necessary to obtain more knowledge of the iron oxide's behavior in the chemical-looping hydrogen generation process.

The aim of this work is to present the behavior of oxygen carrier Fe_2O_3 supported on Al_2O_3 or TiO_2 in chemical-looping hydrogen generation process in a batch fluidized bed. It focused on the performance of the oxygen carrier. The reactivity and stability of the oxygen carrier supported on varied materials in multiple cycles were investigated. Carbon

deposition characteristics, sintering and agglomeration were also analyzed in the experiment.

2. Experimental

2.1. Oxygen carrier preparation

The iron oxide oxygen carriers were manufactured by Nanjing Chemical Industry Co. Ltd. It was prepared using mechanical-mixing method. It consisted of Fe_2O_3 with Al_2O_3 or TiO_2 as supports. The Al_2O_3 or TiO_2 supports play an important role here to maintain the constant reactivity and the mechanical strength of the oxygen carrier over multiple cycles. Three oxygen carriers, named Fe90Al10, Fe60Al40 and Fe60Ti40, were produced for the experiment. Fe, Al and Ti were the abbreviations of Fe_2O_3, Al_2O_3 and TiO_2. The number behind the letter was the mass fraction of each component, thus for Fe90Al10 the mass ratio of Fe_2O_3 and Al_2O_3 was 90% and 10%, respectively. The oxygen carrier pellets were crushed and sieved to a size range of 200–300 μm for the fluidized bed experiment; the residual powder less than 90 μm was used in the TGA test.

2.2. Redox in TGA

Before the experiments in a fluidized bed, the reactivity of oxygen carrier was determined in a thermogravimetric analyzer, TherMax 500 by Thermo Cahn Co. Ltd. A sample of 20 mg of oxygen carrier was loaded in a platinum basket in a quartz reactor and heated to the set operation temperature up to 900 °C in a nitrogen atmosphere. The heating rate was 25 °C/min. The total flow of nitrogen was 270 ml/min for all periods. The sample was first exposed to a reducing gas for 30 min. The composition of the gas selected in the reduction period was composed of 10% CO and 90% N_2; secondly, the reduced sample was oxidized with 65% H_2O and 35% N_2 for 15 min; finally the sample was exposed to 10% O_2 and 90% N_2 for 15 min. To avoid mixing of gases in each phase, nitrogen was introduced for 5 min after each reaction period. The sample was exposed periodically to reducing and oxidizing conditions for 3 cycles.

To facilitate a comparison between different oxygen carriers that contain varying amounts of oxygen depending upon the fraction of inert, a mass-based conversion was defined:

$$\omega = \frac{m}{m_{ox}} \times 100\% \tag{1}$$

Where m is the actual mass of sample, m_{ox} is the mass of the sample when fully oxidized, i.e., $Fe_2O_3 + Al_2O_3/TiO_2$.

To characterize the molar fractions of Fe and FeO in the residual solids sample after reduction in TGA, a set of equations are listed below based on mass balance and element conservation:

$$\begin{cases} n_{Fe} + n_{FeO} = 2m_{ox}f_{Fe_2O_3}/M_{Fe_2O_3} \\ M_{Fe}n_{Fe} + M_{FeO}n_{FeO} + m_{ox}f_{inert} = \omega_r m_{ox} \\ f_{Fe_2O_3} + f_{inert} = 1 \end{cases} \tag{2}$$

Where n_{Fe} is the moles of metallic iron Fe, n_{FeO} is the moles of wüstite FeO, and m_{ox} is the mass of oxygen carrier used in experiment; M_{Fe}, M_{Feo} and $M_{Fe_2O_3}$ is the molar mass of Fe, FeO and Fe_2O_3, respectively; ω_r is the mass-based conversion at the end of reduction; $f_{Fe_2O_3}$ and f_{inert} are the mass fractions of Fe_2O_3 and inert support in the prepared oxygen carriers. Therefore, the molar fraction of Fe or FeO in the product solid after reduction can be easily calculated from the equations above.

2.3. Experiments in a fluidized bed

Fig. 2 shows the experimental setup used for testing the oxygen carriers. It consisted of a fluidized bed reactor (i.d. 40 mm, H1600 mm), an oxygen carrier feeding unit, a gas purification unit, a data acquisition system, and a temperature control section. The preheated fuel gas entered the reactor in the lower conically shaped part of the reactor and the oxygen carrier was blown to the reactor in the lower part of the reactor through nitrogen. Temperature sensors and differential pressure indicators were located along the reactor. Additional temperature sensors were installed to measure the temperature in the center of the fluidized bed. The reactor was heated by electrical oven and maintained at a given temperature through the control system. Gases from the reactor passed through a small cyclone to separate small particles. The amount of particles collected in the cyclone was measured after each experiment. Then the gas was led to a cooler and a dryer, where the residual steam vapor in the product gas was absorbed. Eventually the dry product gas was measured by a flow meter. The gases from the fluidized bed were not monitored in real time but were collected by sample bags every 2 min. Finally the gases were analyzed by Emerson gas analyzers including a Rosemount NGA 2000 gas analyzer used to measure the concentrations of O_2, CO, CO_2, CH_4, and a Hydro100 analyzer to detect the concentration of H_2. The full scales of O_2, CO, CO_2, CH_4 and H_2 were 0–25%, 0–100%, 0–100%, 0–10% and 0–50%, respectively. The uncertainties

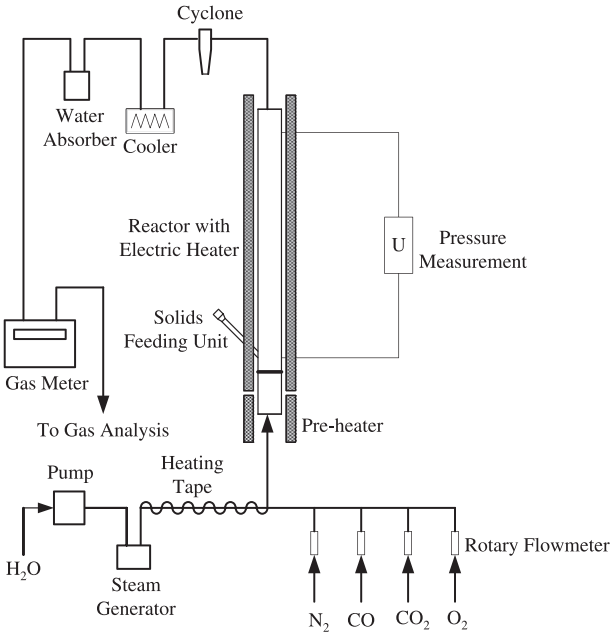

Fig. 2 – Schematic layout of the laboratory setup.

were ±0.1% for H_2 and ±0.01% for other gases from the readout of the gas analyzers.

The experiments were carried out at 600–900 °C. The composition of the gas was 120 L/h CO + 200 L/h N_2 during reduction (u/u_{mf} = 4.8), 12.5 ml/min H_2O (l) + 200 L/h N_2 (u/u_{mf} = 23) during steam oxidization and 60 L/h O_2 + 300 L/h N_2 (u/u_{mf} = 5.3) during the air oxidation. To avoid mixing of gases in different phases, N_2 was introduced for 5 min after each reducing, steam oxidizing and air oxidizing period.

2.4. *Characterization of oxygen carriers*

The morphological features of iron oxide samples before and after multi-cycle experiments were characterized by a scanning electron microscope (SEM, Sirion). To determine the chemical transformations which occurred in the samples after multiple cycles, an X-ray diffractometer (D/max 2500/PC, Japan Rigaku Corp.) using Cu Kα radiation (40 kV and 200 mA) was used to analyze the samples. The samples were scanned in a step-scan mode, with a step size of 0.02° over the angular 2θ range of 5–85°. The surface area of the oxygen carrier was also determined by the BET method and measured through nitrogen adsorption/desorption at 77 K by a Micromeritics analyzer, ASAP 2020.

3. Results and discussion

3.1. *Thermogravimetric experiments*

The reactivity of the three oxygen carriers was firstly evaluated in TGA. The experimental series performed in TGA consisted of 3 redox-cycle experiments. The variation of weight percentage of oxygen carrier with time in the experiments is shown in Fig. 3. The curves trends of the three oxygen carriers were nearly the same. Compared to the slow reaction rate in the reduction period, the steam oxidation and air oxidation were very fast with a sharp rising in the signals of weight. It indicated that the steam oxidation was not the time-consuming step as the air oxidation. The reactivity of the oxygen carrier was different in the first cycle and then stabilized in the later two cycles; it can be speculated that the particles need one cycle to attain a more favorable structure. In the cycles, the air oxidation peaks diminished slightly, especially for Fe60Ti40, suggesting a decrease in reactivity of the oxygen carrier. Taking the second reduction in the cycles to calculate the mass fractions of residual solids, the weight at the initial stage of the second reduction was defined as 100%. Among the three oxygen carriers, Fe90Al10 had the largest weight loss in the reduction. Its weight percentage was around 86.2% at the end of the reduction, but it was not suggesting its best reactivity among the three oxygen carriers. For Fe90Al10, if all of the elemental Fe was reduced to metallic iron, the weight percentage would be approximately 73%, which was the largest weight loss in theory; if all of the elemental Fe was reduced to FeO, the weight percentage would be 91%. In this experiment, the lowest weight percentage was approximately 86.2%, indicating the reduced solids were between Fe and FeO. Metallic iron Fe had a molar fraction of 26.7% and wüstite FeO had a fraction of 73.3%. It

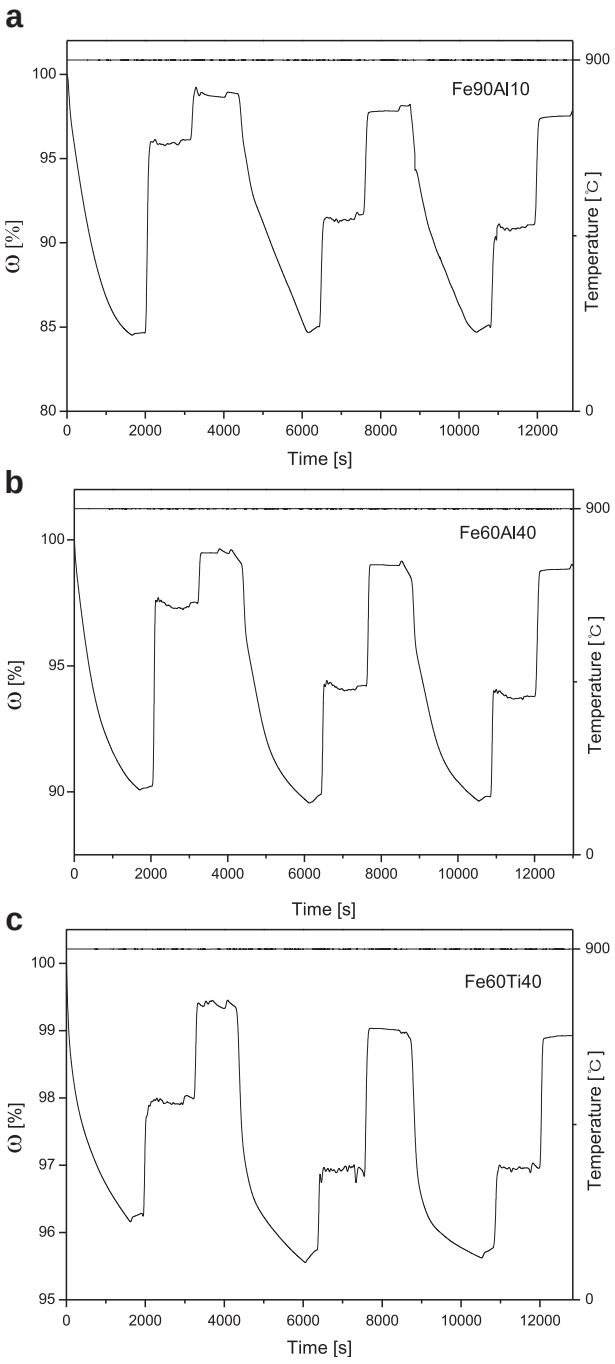

Fig. 3 – Weight percentage of (a) Fe90Al10, (b) Fe60Al40 and (c) Fe60Ti40 as a function of number of redox cycles at 900 °C at TGA.

was not excluded that some local sites were only reduced to magnetite Fe_3O_4 in the core of some particles. For hematite supported on 40% inert materials, i.e., Fe60Al40 and Fe60Ti40, the weight percentage would be 82%, 94% and 98% for a reduced solids product of Fe, FeO and Fe_3O_4. In Fig. 3, the weight losses of Fe60Al40 and Fe60Ti40 were obviously smaller than that of Fe90Al10. The lowest weight percentage in the second reduction for Fe60Al40 and Fe60Ti40 was appropriately at 89.8% and 96.2%, respectively. From the

weight loss it can be deduced that Fe60Al40 was also reduced to FeO and Fe with a fraction of metallic iron 34.3% and wüstite 65.7%, which had more amount of reduced metallic iron than Fe90Al10. For Fe60Ti40, little metallic iron Fe was the solid product, nearly all of the elemental iron was in the form of FeO and Fe_3O_4. It indicated that the reactivity of Fe60Ti40 was lower than that of Fe90Al10 and Fe60Al40. From the TGA experiment, Fe60Al40 showed the highest reactivity among the three oxygen carriers. For Fe60Ti40, $FeTiO_3$ may be formed at a high temperature during reduction. $FeTiO_3$ is a spinel in which Fe^{2+} ion is stabilized against reduction and oxidation. The $FeTiO_3$ formation in Fe60Ti40 also contributed to lower reactivity compared with oxygen carriers supported on Al_2O_3. The reactivity of the oxygen carrier can be identified in the TGA, complete assessment of oxygen carrier performance, however, should be obtained from multi-cycle fluidized bed experiments.

3.2. *Multi-cycle experiments in the fluidized bed*

Chemical-looping hydrogen generation process was simulated in the fluidized bed by alternating the gas atmosphere of the reactor. In the multi-cycle experiments, the solid inventory in the reactor for Fe90Al10, Fe60Al40 and Fe60Ti40 was 20, 30 and 30 g to guarantee the same amount of active Fe_2O_3 for comparison. The reduction period was 30 min. Even though the steam oxidation rate is much higher than that of reduction, the time of steam oxidation was set as long as 15 min for a full conversion FeO/Fe to Fe_3O_4. Each oxygen carrier was run for approximately 17 h at 900 °C.

Fig. 4a shows the effluent gas concentrations as a function of time for a typical steam oxidation in a cycle of Fe60Al40 at 900 °C. Hydrogen was generated as steam was supplied into the reactor. At the first point, gas concentrations were rather low due to the dilution of the residual nitrogen in the fluidized bed reactor. During steam oxidation, CO and CO_2 were detected in the hydrogen stream, indicating carbon deposition occurred in the reduction period. The hydrogen peak was 18.8 vol% at the third point. The purity of produced hydrogen on nitrogen-free base at this maximum hydrogen concentration was 97.0%. As the reaction proceeded, the hydrogen concentration declined with the consumption of FeO and Fe. The analysis of carbon deposition will be discussed in the later section.

Fig. 4b shows the cumulative amount of hydrogen generated in the steam oxidation period as a function of the number of cycles. It is clear that the amount of hydrogen generated was highest for Fe60Al40, and there were few differences in the yields achieved by Fe90Al10 and Fe60Ti40. The state of reduced sample solids could be deduced from the amount of hydrogen obtained in the steam oxidation period. In the reduction periods, all of the oxygen carriers were reduced to a range between FeO and Fe. For Fe60Al40, more metallic iron Fe was obtained, and it generated more hydrogen in the following steam oxidation period. The observation also suggests that the support material could markedly affect the reactivity of an oxygen carrier. The ability of oxygen carrier to generate hydrogen is associated with the active site FeO/Fe on the particles. The theoretical amount of Fe_2O_3 in these three oxygen carrier was the same, but for Fe60Al40, there were more support materials and more active iron oxide sites were

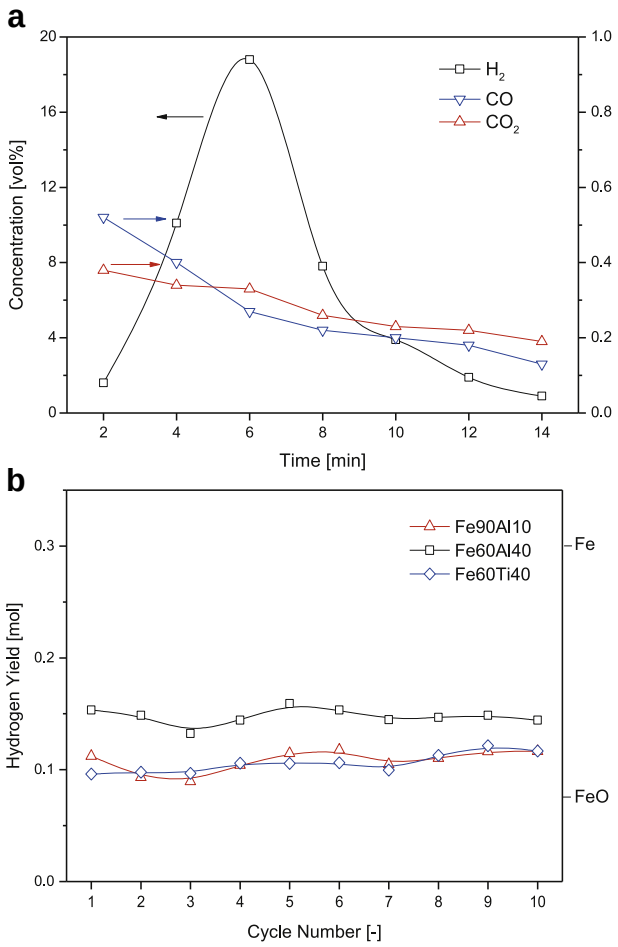

Fig. 4 – (a) The effluent gas concentrations as a function of time for a typical steam oxidation in a cycle of Fe60Al40 at 900 °C; (b) Performance of Fe90Al10, Fe60Al40 and Fe60Ti40 particles over 10 cycles.

dispersed on the per unit support area relatively. The accessibility of the reactant gases to the metal oxide was increased. More oxygen was available on this support during reduction. However, for Fe90Al10 and Fe60Ti40, a deeper combination between Fe_2O_3 and Al_2O_3 or TiO_2 may lead to the formation of spinel like $FeAl_2O_4$ [48] or $FeTiO_3$, which is less reductive than Fe_2O_3. The available oxygen in these supports was less than the one theoretically expected given the formation of the spinel. Therefore, the reactivity of oxygen carrier Fe60Al40 was the best among the three oxygen carriers; the oxygen carrier supported on less inert materials had potential to agglomerate, which will be discussed in the later section. In general, the reactivity of the oxygen appeared constant from cycle to cycle, and no loss of reactivity was detected during the test period.

The identification of crystalline phases of the reacted oxygen carriers has been determined by powder XRD as shown in Table 1. Alumina used as support was microcrystalline giving diffuse X-ray patterns in opposition to hematite and titania that present very intense reflections allowing easy identification. Interestingly, goethite FeO(OH) was found in all of the three oxygen carriers after multi-cycle experiments.

Table 1 – BET surface area of the sample particles and main crystalline phase before and after the multi-cycle experiments.

Sample particles	BET surface area (m^2/g)	Main crystalline phase
Fe90Al10 (fresh)	65.6	Fe_2O_3, Al_2O_3(trace)
Fe90Al10 (reacted)	50.3	Fe_2O_3, FeO(OH), Al_2O_3(trace)
Fe60Al40 (fresh)	143.0	Fe_2O_3, Al_2O_3
Fe60Al40 (reacted)	100.7	Fe_2O_3, FeO(OH), Al_2O_3, AlO(OH)
Fe60Ti40 (fresh)	47.75	Fe_2O_3, TiO_2
Fe60Ti40 (reacted)	37.17	Fe_2O_3, $FeTiO_3$, FeO(OH), TiO_2

FeO(OH) is the hydroxide of iron oxide, it is a combination of Fe_2O_3 and H_2O. For Fe90Al10 and Fe60Al40, no spinel-structure $FeAl_2O_4$ was detected after cycles as expected but for Fe60Ti40, the spinel-structure $FeTiO_3$ was evidenced in the residual samples, confirming there was an interaction between the active phase and the support TiO_2 through the formation of this mixed solid solution [49], which decreased the reactivity of the oxygen carrier. In the sample specimen of Fe60Al40, which contains more fraction of Al_2O_3, a few boehmite AlO(OH) was also detected after multi-cycle experiments. The phenomena indicated that in the atmosphere of steam vapor, the water molecule was prone to be absorbed and interacted with the metal oxide like Fe_2O_3 or Al_2O_3, forming its hydrate; however, the detailed route of this hydrate formation is not clear. Table 1 also illustrates the changes in the BET surface area of the sample particles before and after the multi-cycle experiments. Fe60Al40 had a much higher surface area than other two sample particles. Higher surface area of Fe60Al40 increased the accessibility of the reactant gases to the metal oxide, which also suggested its best reactivity among the three oxygen carriers. All of the three oxygen carriers had a decrease in the surface area after cycles, especially for Fe60Al40, but fortunately, they didn't deactivate the reactivity of the oxygen carriers, as shown in Fig. 4b. The variation of surface area suggested that the oxygen carrier supported on Al_2O_3 gave a higher porosity and surface area than that on TiO_2.

3.3. *Influence of temperature*

Fig. 5 shows the cumulative amount of hydrogen generated at varied temperatures in the 600–900 °C. The oxygen carrier used in the experiments was Fe60Al40. The solid inventory was 30 g and particle size was 200–300 μm. At each temperature, five consecutive redox cycles were performed. It can be observed that the hydrogen yield was obviously dependent on temperature. At higher temperature, the hydrogen yield was higher. In the chemical-looping hydrogen generation system, there are two processes which have the potential to influence the hydrogen yield, i.e., the reduction process and the following steam oxidation process. In order to generate hydrogen, the solid particles must be reduced to wüstite FeO or metallic iron Fe in the reduction period. The global reduction of Fe_2O_3 to FeO or Fe is endothermic. On the contrary, the steam oxidation is

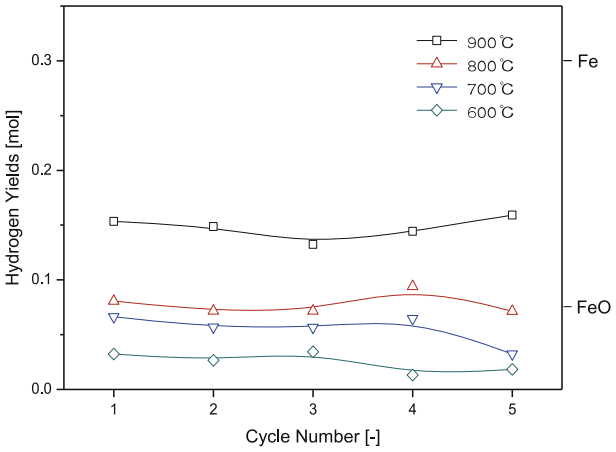

Fig. 5 – Performance of Fe60Al40 at varied temperature over 5 cycles.

exothermic; the hydrogen equilibrium constant is higher at lower temperatures. In the experiment, the temperature adopted in the steam oxidation phase had only a limited impact on the total hydrogen yield. The capacity of CLHG to generate hydrogen is associated with the amount of reductive wüstite FeO and metallic iron Fe. Even though the steam oxidation reaction rate decreases at lower temperatures, the steam oxidation rate is intrinsically high in kinetics and in this experiment the steam oxidation period was long enough. Thus the temperature adopted in the steam oxidation could not affect the total hydrogen yield. However, the reduction of Fe_2O_3 to FeO or metallic iron Fe is strongly limited by thermodynamics and kinetics. It has been confirmed that hematite Fe_2O_3 reduction to magnetite Fe_3O_4 is the fast step with the subsequent steps, magnetite Fe_3O_4 to wüstite FeO and wüstite to metallic iron Fe, being much slower [12]. From the point of view of thermodynamics, high temperature favors the equilibrium to the product side in the reduction; more importantly, the reduction rate was enhanced by kinetics at high temperature and more amounts of reductive products FeO or Fe was obtained in a fixed period, which directly increased the hydrogen yield in the following step.

3.4. *Carbon deposition*

Thermodynamically it is possible that carbon is deposited on the surface of solid carrier when iron oxide is reduced by carbonaceous fuels. In chemical-looping hydrogen generation, the carbon deposition on the solid carrier limits the efficiency of the total carbon dioxide capture. Furthermore, the carbon deposited in the fuel reactor can be transferred to the steam reactor along with oxygen carrier, and reoxidized to carbon monoxide and carbon dioxide, decreasing the hydrogen purity. Boudouard reaction is among the most probable reactions leading to carbon deposition:

$$2CO \leftrightarrow C + CO_2$$

The solid carbon then reacted with steam and CO was generated according to:

$C + H_2O \leftrightarrow H_2 + CO$

Also, shift reaction could occur, releasing CO_2:

$CO + H_2O \leftrightarrow H_2 + CO_2$

Fig. 6a shows average $CO + CO_2$ concentration in the steam oxidation for Fe90Al10, Fe60Al40 and Fe60Ti40 in multi-cycle experiments at 900 °C. It is obvious that carbon deposition occurred during reduction period. Kinetically, Boudouard reaction is known to have a limited importance in the absence of a catalyst. However, metallic site such as Fe could act as a catalyst. Cho et al. [50] reported that for oxygen carrier based on nickel oxide carbon formation is strongly dependent on the oxygen availability. Rapid carbon formation starts when more than 80% of the available oxygen carrier is consumed; for particles with iron oxide, no or very little carbon was formed. The result is different from this study. There are two interpretations. Firstly, in CLC the reduced solid product is magnetite Fe_3O_4 pursuing a full conversion of fuels, whereas in this experiment the reduced solids were mostly wüstite FeO or metallic iron Fe for hydrogen generation, where less oxygen was available. The active crystalline site of wüstite and metallic iron played a role of catalyst, and carbon deposition on the surface of iron oxide oxygen carrier started as wüstite or metallic iron was produced [51]; secondly, the reduction period in this study was so long to get a solid conversion to wüstite and metallic iron, thus more deposited carbon was obtained due to accumulation. In the air oxidation, CO and CO_2 were also detected. The amount of CO and CO_2 was low compared with that in the steam oxidation period. Much of the deposited carbon had been consumed in the steam oxidation. The amount of the deposited carbon varied little with Fe90Al10, Fe60Al40 and Fe60Ti40. It is not obvious of the relationship between carbon deposition with different supports and contents in this experiment, and further research is needed.

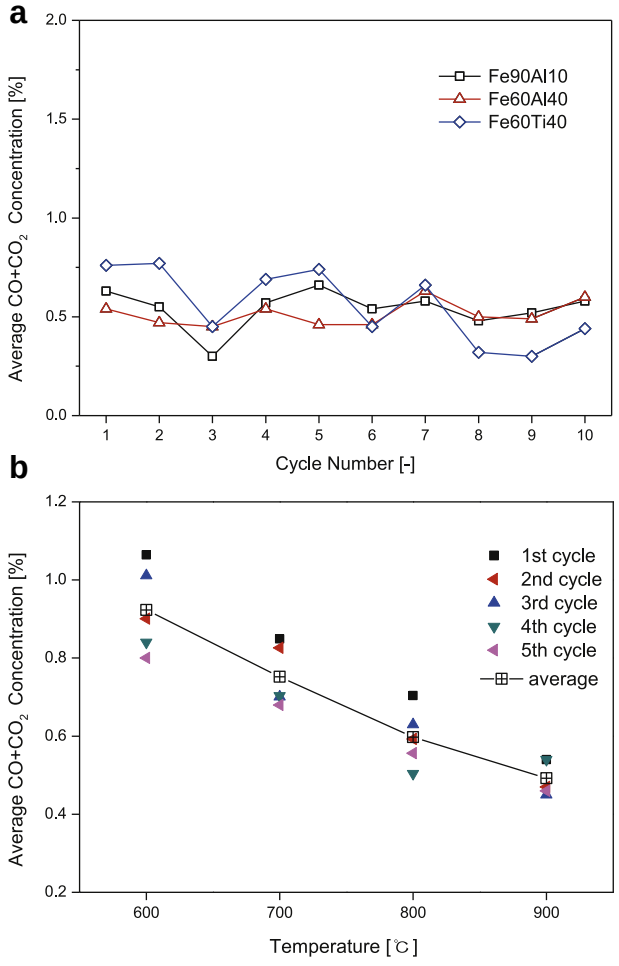

Fig. 6 – (a) The average CO + CO_2 concentration released in the steam oxidation period over cycles with different oxygen carriers at 900 °C; (b) the average CO + CO_2 concentration released in the steam oxidation period for Fe60Al40 over 5 cycles at 600–900 °C.

The average $CO + CO_2$ concentration for Fe60Al40 in the steam oxidation period at different temperatures is illustrated in Fig. 6b. It is seen that the amount of carbon deposited was correlated to temperature. More deposited carbon was formed at lower temperatures. This is simply explained by Boudouard reaction. The Boudouard reaction is exothermic, lower temperature favored this carbon deposition. Less CO and CO_2 were detected during steam oxidation at higher temperature. In actual application of the process, within the thermal tolerance of the oxygen carrier, the temperature of the fuel reactor would be run as high as possible for kinetics; moreover, the addition of steam into the fuel reactor is also an efficient way to alleviate the carbon formation [48], thus the purity of hydrogen produced could be enhanced, which decreases the energy penalties in further purification devices.

3.5. *Morphology and agglomeration*

The SEM images of surface morphology of fresh and reacted samples after ten redox cycles at 900 °C are shown in Fig. 7. For the three oxygen carriers, the presence of holes or cracks was evident and the general appearance of the reacted particles was similar to the fresh particles. No sintering occurred on the surface of the oxygen carriers, but thermal sintering may occur in the inner pores because the surface area of the particles had a decrease as shown in Table 1. Interestingly, the particle size was obviously larger than the original ones and showed slight agglomeration in the reactor, especially for Fe90Al10. Small solid lumps were detected during removing the particles Fe90Al10 from the reactor. It was shown in Fig. 8. The agglomerates were very small, ~2–3 mm, and were so soft that they could easily be crushed to powder by fingers. From the morphology and mechanical strength of the particles and agglomerates, it suggests that two aspects may lead to agglomeration. The first is the molten material that fused together during reaction. Fe90Al10 contains the least inert to support active crystallites. The reduced crystalline cluster was denser and tended to agglomerate. The second is the interaction between particles and humid atmosphere. After the experiment, the reactor was purged by nitrogen to room temperature. The residual steam in the reactor condensed and mixed with particles, after drying, solid lumps were formed. This formation of agglomerates was inevitable in such

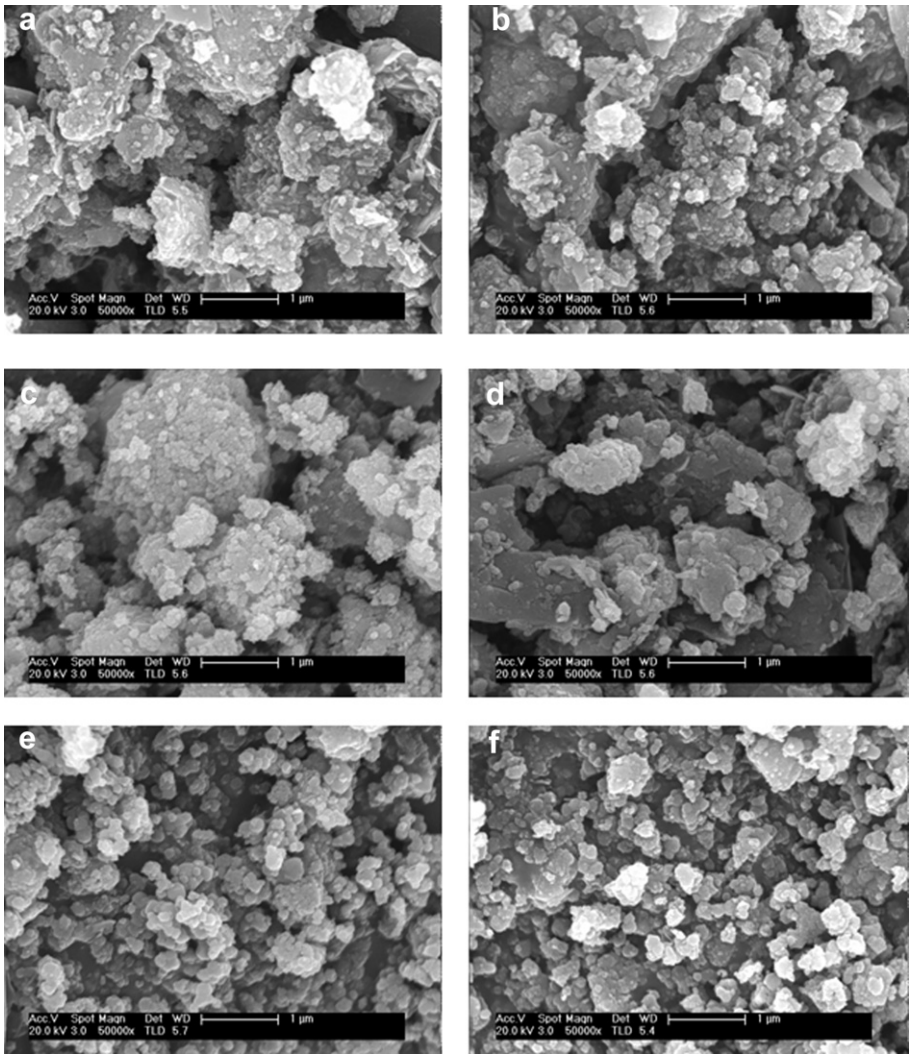

Fig. 7 – SEM images of the fresh and the reacted oxygen carrier particles after multi-cycle experiments (a) fresh Fe90Al10; (b) reacted Fe90Al10; (c) fresh Fe60Al40; (d) reacted Fe60Al40; (e) fresh Fe60Ti40; (f) reacted Fe60Ti40.

a humid atmosphere. It is worthwhile to note that in an actual chemical-looping hydrogen generation pilot, the second reason can be avoided during normal operation but can not be neglected in the downtime. So much oxygen carrier stacks in the steam reactor, mixes with the residual water and agglomerates together, which may block the reactor. For the first aspect, it can be concluded that more support material can improve the ability of the oxygen carrier against agglomeration.

3.6. *Fuel conversion*

To obtain a pure stream of CO_2 at the outlet of the fuel reactor, it is necessary to get a full conversion of the fuel gas. In CLC with iron oxide as oxygen carrier, the circulating solids between the two reactors are Fe_2O_3 and Fe_3O_4. In the fuel reactor, the reduced solid is Fe_3O_4. Any deeper reduction of Fe_3O_4 would lead to unconverted fuel gas escaping from the fuel reactor because of thermodynamic equilibrium. However, in chemical-looping hydrogen generation, the solids must be reduced to FeO or Fe for hydrogen generation. A typical reduction period of Fe60Al40 in the multi-cycle experiments is shown in Fig. 9. At the initial stage of reduction, one can observe a breakthrough of CO after a CO_2 peak. The CO_2 peak resulted from the fast reduction of Fe_2O_3 to Fe_3O_4, which can get a nearly full conversion (~99.995% at 900 °C in theory) of CO to CO_2. As the reaction proceeded, Fe_2O_3 disappeared due to particle reduction. The reduction of Fe_3O_4 and FeO is reversible and gives incomplete conversion of fuels, thus much of CO left the reactor without reacting. The full conversion of gaseous fuels can not be achieved in a single-stage reactor.

To get a full conversion of gaseous fuels, a novel fuel reactor is proposed here as shown in Fig. 10. The configuration can be found elsewhere [46]. It is a compact fluidized bed reactor. It consists of a bubble fluidized bed, a riser, a cyclone and a dipleg. Fe_2O_3 flows along the riser upward and is reduced to Fe_3O_4 by unburned fuel gas from the bubbling fluidized bed below, the product gases are primarily CO_2 and H_2O. After water condensation, pure CO_2 can be obtained. Fe_3O_4 then falls into

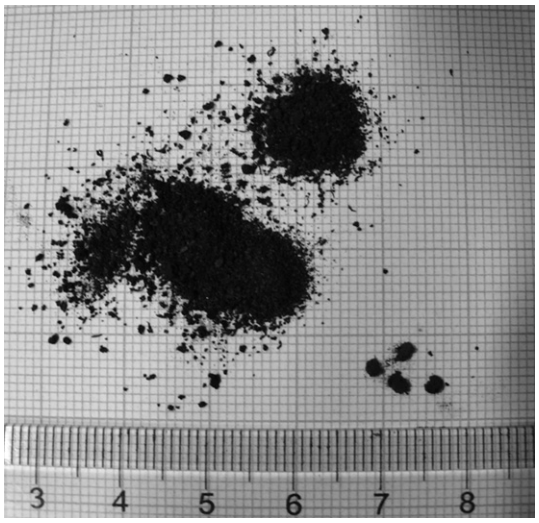

Fig. 8 – Photograph of residual solids collected after multi-cycle experiments for Fe90Al10.

the bubble fluidized bed and is further reduced to FeO or Fe for hydrogen generation. The unburned fuel gases from the bubbling fluidized bed enter into the upper riser, converting Fe_2O_3 to Fe_3O_4. Through the compact fuel reactor, FeO or Fe is obtained with a full conversion of fuel gases.

Here, Fe_2O_3 is added into the effluent gases from reduction of Fe_3O_4 to FeO/Fe in the bubble fluidized bed, polishing the unreacted CO and H_2 and getting a complete conversion of the gaseous fuels. Fe_2O_3 is from the reoxidation of Fe_3O_4. Owing to thermodynamic constraints, the direct oxidation of Fe_3O_4 to Fe_2O_3 with steam is impossible ($P_{H_2O}/P_{H_2} > 10^4$, 900 °C), preventing the transition from Fe_3O_4 to Fe_2O_3 in the steam reactor. Therefore, air has to be used to regenerate Fe_3O_4 to Fe_2O_3. That's why there are three reactors in the chemical-looping hydrogen generation and a compact fuel reactor is required. Besides the proposed compact fluidized fuel reactor, previous investigation recommended that reactant gases

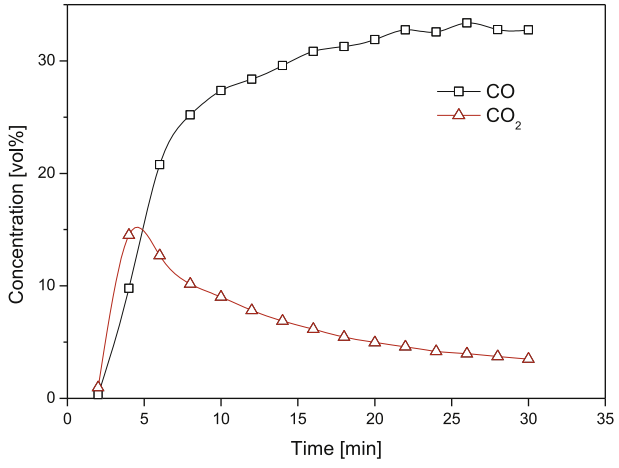

Fig. 9 – Typical product gas distribution in the reduction period of a cycle for Fe60Al40 oxygen carrier during multi-cycle experiments in the fluidized bed.

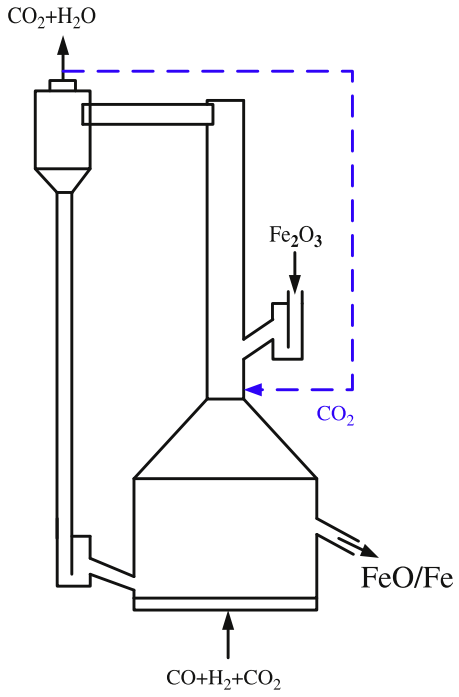

Fig. 10 – The proposed compact fuel reactor for chemical-looping hydrogen generation.

could come in contact with a high oxidation state oxygen carrier before exiting the fuel reactor. A moving bed or multistage fluidized bed would be also suitable as a fuel reactor [32,35,36].

4. Conclusions

Three oxygen carriers Fe_2O_3 supported on Al_2O_3 and TiO_2 were prepared by mechanical-mixing method. The reactivity of sample particles was tested in TGA. Multi-cycle experiments were also performed to investigate the reactivity, recyclability and stability of the oxygen carrier for chemical-looping hydrogen generation.

Using Al_2O_3 as support material, the reactivity of oxygen carrier was higher with the increase of mass fraction of Al_2O_3 in the oxygen carrier. With the same amount of support, the reactivity of the oxygen carrier supported on Al_2O_3 was better than TiO_2 because Al_2O_3 gave a more porous structure and a higher surface area for reaction.

At 900 °C, for each oxygen carrier, the hydrogen production varied little over ten cycles and there was no deactivation of the oxygen carrier, but the surface areas of the oxygen carriers had a decrease. For iron oxide supported on 40% TiO_2, $FeTiO_3$ were formed. Some hydrates FeO(OH) and AlO(OH) were also detected. The SEM images showed the morphology of the oxygen carrier had not changed after cycles. However, agglomeration was detected. Agglomeration may derive from two sources: one was the fusion of the metal; the other was the mixing with water in humid atmosphere in the reactor.

Higher temperature increased the hydrogen yield because higher temperature favored deeper reduction of iron oxide

and more reductive solids were obtained. Carbon deposition occurred in the reduction and CO and CO_2 were detected during the steam oxidation. Lower temperature favored the carbon deposition. Much of the deposited carbon was consumed in the steam oxidation phase, only a little CO or CO_2 were detected in the air oxidation phase.

Acknowledgments

The authors gratefully acknowledge the National Natural Science Foundation of China (50776018) and the Special Fund of the National Priority Basic Research of China (2007CB210101) for financial support of this project.

REFERENCES

[1] Kothari R, Buddhi D, Sawhney R. Comparison of environmental and economic aspects of various hydrogen production methods. Renewable and Sustainable Energy Reviews 2008;12:553–63.
[2] Word coal institute. Available from: http://www.worldcoal.org/coal/.
[3] Cormos C, Starr F, Tzimas E, Peteves S. Innovative concepts for hydrogen production processes based on coal gasification with CO_2 capture. International Journal of Hydrogen Energy 2008;33:1286–94.
[4] Cormos C, Starr F, Tzimas E. Use of lower grade coals in IGCC plant with carbon capture for the co-production of hydrogen and electricity. International Journal of Hydrogen Energy 2010;35:556–67.
[5] Johansson E, Mattisson T, Lyngfelt A, Thunman HA. 300 W laboratory reactor system for chemical-looping combustion with particle circulation. Fuel 2006;85:1428–38.
[6] Linderholm C, Mattisson T, Lyngfelt A. Long-term integrity testing of spray-dried particles in a 10-kW chemical-looping combustor using natural gas as fuel. Fuel 2009;88:2083–96.
[7] Forero C, Gayán P, de Diego L, Abad A, García-Labiano F, Adánez J. Syngas combustion in a 500 Wth chemical-looping combustion system using an impregnated Cu-based oxygen carrier. Fuel Processing Technology 2009;90:1471–9.
[8] Adánez J, Dueso C, de Diego L, García-Labiano F, Gayán P, Abad A. Methane combustion in a 500 Wth chemical-looping combustion system using an impregnated Ni-based oxygen carrier. Energy & Fuels 2009;23:130–42.
[9] Shen LH, Wu JH, Xiao J. Experiments on chemical looping combustion of coal with a NiO based oxygen carrier. Combustion and Flame 2009;156:721–8.
[10] Shen LH, Wu JH, Gao ZP, Xiao J. Reactivity deterioration of NiO/Al_2O_3 oxygen carrier for chemical looping combustion of coal in a 10 kWth reactor. Combustion and Flame 2009;156:1377–85.
[11] Lyngfelt A, Johansson M, Mattisson T. Chemical-looping combustion-status of development. 9th international conference on circulating fluidized beds, Hamburg, Germany; 2008.
[12] Hossain M, de Lasa H. Chemical-looping combustion (CLC) for inherent CO_2 separations-a review. Chemical Engineering Science 2008;63:4433–51.
[13] Shulman A, Cleverstam E, Mattisson T, Lyngfelt A. Manganese/iron, manganese/nickel, and manganese/silicon used in chemical-looping with oxygen uncoupling (CLOU) for combustion of methane. Energy & Fuels 2009;23:5269–75.
[14] Mattisson T, Lyngfelt A, Leion H. Chemical-looping with oxygen uncoupling for combustion of solid fuels. International Journal of Greenhouse Gas Control 2009;3:11–9.
[15] Leion H, Larring T, Bakken E, Bredesen R, Mattisson T, Lyngfelt A. Use of $CaMn_{0.875}Ti_{0.125}O_3$ as oxygen carrier in chemical-looping with oxygen uncoupling. Energy & Fuels 2009;23:5276–83.
[16] Mattisson T, Leion H, Lyngfelt A. Chemical-looping with oxygen uncoupling using CuO/ZrO_2 with petroleum coke. Fuel 2009;88:683–90.
[17] de Diego L, Ortiz M, Adánez J, García-Labiano F, Abad A, Gayán P. Synthesis gas generation by chemical-looping reforming in a batch fluidized bed reactor using Ni-based oxygen carriers. Chemical Engineering Journal 2008;144:289–98.
[18] Rydén M, Lyngfelt A, Mattisson T, Chen D, Holmen A, Bjørgum E. Novel oxygen-carrier materials for chemical-looping combustion and chemical-looping reforming; $La_xSr_{1-x}Fe_yCo_{1-y}O_{3-\delta}$ perovskites and mixed-metal oxides of NiO, Fe_2O_3 and Mn_3O_4. International Journal of Greenhouse Gas Control 2008;2:21–36.
[19] Rydén M, Lyngfelt A, Mattisson T. Chemical-looping combustion and chemical-looping reforming in a circulating fluidized-bed using Ni-based oxygen carriers. Energy & Fuels 2008;22:2585–97.
[20] Ortiz M, de Diego L, Abad A, García-Labiano F, Gayán P, Adánez J. Hydrogen production by auto-thermal chemical-looping reforming in a pressured fluidized bed reactor using Ni-based oxygen carriers. International Journal of Hydrogen Energy 2010;35:151–60.
[21] de Diego L, Oritiz M, García-Labiano F, Adánez J, Abad A, Gayán P. Hydrogen production by chemical-looping reforming in a circulating fluidized bed reactor using Ni-based oxygen carriers. Journal of Power Sources 2009;192:27–34.
[22] Pröll T, Bolhàr-Nordenkampf J, Kolbitsch P, Hofbauer H. Syngas and a separate nitrogen/argon stream via chemical looping reforming-a 140 kW pilot plant study. Fuel 2010;89:1249–56.
[23] Mattison T, Lyngfelt A. Applications of chemical-looping combustion with capture of CO_2. Proceedings of the 2nd Nordic minisymposium on carbon dioxide capture and storage, Göteborg, Sweden; 2001.
[24] Rydén M, Lyngfelt A, Mattisson T. Synthesis gas generation by chemical-looping reforming in a continuously operating laboratory reactor. Fuel 2006;85:1631–41.
[25] He F, Wei YG, Li HB, Wang H. Synthesis gas generation by chemical-looping reforming using Ce-based oxygen carriers modified with Fe, Cu, and Mn oxides. Energy & Fuels 2009;23:2095–102.
[26] Zafar Q, Mattisson T, Gevert B. Integrated hydrogen and power production with CO_2 capture using chemical-looping reforming-redox reactivity of particles of CuO, Mn_2O_3, NiO, and Fe_2O_3 using SiO_2 as a support. Industrial & Engineering Chemistry Research 2005;44:3485–96.
[27] Cleeton J, Bohn C, Müller C, Dennis J, Scott S. Clean hydrogen production and electricity from coal via chemical looping: identifying a suitable operating regime. International Journal of Hydrogen Energy 2009;34:1–12.
[28] Gnanapragasam N, Reddy B, Rosen M. Hydrogen production from coal using coal direct chemical looping and syngas chemical looping combustion systems: assessment of system operation and source requirements. International Journal of Hydrogen Energy 2009;34:2606–15.
[29] Jin GT, Ryu HJ, Jo SH, Lee SY, Son SR, Kim SD. Hydrogen production in fluidized bed by chemical-looping cycle. Korean Journal of Chemical Engineering 2007;24:542–6.
[30] Svoboda K, Siewiorek A, Baxter D, Rogut J, Pohořelý M. Thermodynamic possibilities and constraints for pure

hydrogen production by a nickel and cobalt-based chemical looping process at lower temperatures. Energy Conversion and Management 2008;49:221–31.
[31] Son SR, Go KS, Kim SD. Thermogravimetric analysis of copper oxide for chemical-looping hydrogen generation. Industrial & Engineering Chemistry Research 2009;48:380–7.
[32] Kang KS, Kim CH, Bae KK, Cho WC, Kim SH, Park CS. Oxygen-carrier selection and thermal analysis of the chemical-looping process for hydrogen production. International Journal of Hydrogen Energy 2010;35:12246–54.
[33] Gupta P, Velazquez-Vargas L, Fan LS. Syngas redox (SGR) process to produce hydrogen from coal derived syngas. Energy & Fuels 2007;21:2900–8.
[34] Li FX, Kim HR, Sridhar D, Wang F, Zeng L, Chen J, et al. Syngas chemical looping gasification process: oxygen carrier particle selection and performance. Energy & Fuels 2009;23: 4182–9.
[35] Fan LS, Li FX. Chemical-looping technology and its fossil energy conversion applications. Industrial & Engineering Chemistry Research 2010;49:10200–11.
[36] Fan LS, Li FX, Ramkumar S. Utilization of chemical looping strategy in coal gasification processes. Particuology 2008;6: 131–42.
[37] Solunke R, Veser G. Hydrogen production via chemical looping steam reforming in a periodically operated fixed-bed reactor. Industrial & Engineering Chemistry Research 2010; 49:11037–44.
[38] Hurst S. Production of hydrogen by the steam-iron method. Journal of the American Oil Chemists Society 1939;16:29–36.
[39] Bohn C, Müller C, Cleeton J, Hayhurst A, Davidson J, Scott S, et al. Production of very pure hydrogen with simultaneous capture of carbon dioxide using the redox reactions of iron oxides in packed beds. Industrial & Engineering Chemistry Research 2008;47:7623–30.
[40] Cleeton J, Bohn C, Müller C, Dennis J, Scott S. Different methods of manufacturing Fe-based oxygen carrier particles for reforming via chemical looping, and their effect on performance. Proceedings of the 20th international conference on fluidized bed combustion. Tsinghua University Press. pp. 505–511.
[41] Yang JB, Cai NS, Li ZS. Hydrogen production from the steam-iron process with direct reduction of iron oxide by chemical looping combustion of coal char. Energy & Fuels 2008;22: 2570–9.
[42] Kierzkowska A, Bohn C, Scott S, Cleeton J, Dennis J, Müller C. Development of iron oxide carriers for chemical looping combustion using sol-gel. Industrial & Engineering Chemistry Research 2010;49:5383–91.
[43] Chen SY, Xiang WG, Xue ZP, Sun XY. Experimental investigation of chemical looping hydrogen generation using iron oxides in a batch fluidized bed. Proceedings of the Combustion Institute 2011;33:2691–9.
[44] Lozza G, Chiesa P, Romano M, Savoldelli P. Three reactors chemical looping combustion for high efficiency electricity generation with CO_2 capture from natural gas. Proceedings of GT2006, ASME Turbo Expo2006: Power for land, sea and air. Barcelona, Spain; 2006.
[45] Chiesa P, Lozza G, Malandrino A, Romano M, Piccolo V. Three-reactors chemical looping process for hydrogen production. International Journal of Hydrogen Energy 2008; 33:2233–45.
[46] Xiang WG, Chen SY, Xue ZP, Sun XY. Investigation of coal gasification hydrogen and electricity co-production plant with three-reactors chemical looping process. International Journal of Hydrogen Energy 2010;35:8580–91.
[47] Jerndal E, Mattisson T, Lyngfelt A. Thermal analysis of chemical-looping combustion. Chemical Engineering Research and Design 2006;84:795–806.
[48] Svoboda K, Slowinski G, Rogut J, Baxter D. Thermodynamic possibilities and constraints for pure hydrogen production by iron based chemical looping process at lower temperatures. Energy Conversion and Management 2007;48:3063–73.
[49] Son SR, Kim SD. Chemical-looping combustion with NiO and Fe_2O_3 in a thermobalance and circulating fluidized bed reactor with double loops. Industrial & Engineering Chemistry Research 2006;45:2689–96.
[50] Cho P, Mattisson T, Lyngfelt A. Carbon formation on nickel and iron oxide-containing oxygen carriers for chemical-looping combustion. Industrial & Engineering Chemistry Research 2005;44:668–76.
[51] Takenaka S, Hanaizumi N, Son VTD, Otsuka K. Production of pure hydrogen from methane mediated by the redox of Ni- and Cr-added iron oxide. Journal of Catalysis 2004;228: 405–16.